Journal of Hazardous Materials 188 (2011) 198–205

Contents lists available at ScienceDirect

Journal of Hazardous Materials

journal homepage: www.elsevier.com/locate/jhazmat

Selective photocatalytic degradation of aquatic pollutants by titania encapsulated into FAU-type zeolites

Guan Zhang, Wonyong Choi*, Seok Han Kim, Suk Bong Hong

School of Environmental Science and Engineering, Pohang University of Science and Technology (POSTECH), Hyoja-dong, Pohang 790-784, Republic of Korea

ARTICLE INFO

Article history:
Received 20 November 2010
Received in revised form 22 January 2011
Accepted 24 January 2011
Available online 1 February 2011

Keywords:
TiO_2
Zeolite
Photocatalyst
Selective photocatalysis
Water treatment

ABSTRACT

The selective photocatalytic degradation of charged pollutants in water was achieved on titania encapsulated into FAU-type zeolites. The electrostatic attraction of cationic substrates and repulsion of anionic substrates by the negatively charged zeolite framework facilitated the selective photocatalytic degradation of charged substrates. The hybrid zeolite–titania photocatalysts were prepared through the ion-exchange method. The titania clusters were mainly well distributed within the cavities of FAU-type zeolites whereas no TiO_2 nanoparticles aggregates were observed on the external surface of zeolite crystals. The hybrid zeolite–titania photocatalysts were characterized by diffuse reflectance UV–visible spectroscopy, transmission electron microscopy, energy-dispersive X-ray analysis and X-ray photoelectron spectroscopy. The selective degradation of charged pollutants was investigated by employing three pairs of oppositely charged substrates. The comparison between the cationic and anionic substrates clearly showed that the degradation rates for the cationic substrates on the hybrid photocatalysts are markedly higher than those for the anionic substrates. Among the cationic substrates, the smaller cations such as tetramethylammoniums were preferentially degraded. This enabled the selective removal of cationic substrates among the mixture. Such a selective photocatalytic degradation of water pollutants may provide a useful strategy for the development of economical photocatalytic process by targeting only the most recalcitrant pollutant.

1. Introduction

The successful performance of titanium dioxide (TiO_2) photocatalyst has been widely demonstrated especially for the complete mineralization of organic pollutants. The oxidative degradation mediated through the photogenerated hydroxyl radicals and valence band holes with a strong oxidation potential is highly favored and non-selective for a wide range of organic compounds [1–6]. The photocatalysis is environmentally benign because it needs only O_2 and light for generating the reactive oxidants under ambient conditions. However, TiO_2/UV process might be costly for practical water treatment because of the overall low photonic efficiency. Achieving the selective degradation of targeted pollutants among the mixture may enhance the economical feasibility of the photocatalytic process for water treatment. Although the photocatalytic degradation of organic compounds have been extensively studied, the study of the selective degradation among the mixture is rare [7,8]. In general, a combined process can be more efficient and economical than a process that depends on a single technology. When applied to water treatment, photocatalysis may not be efficient if it aims to remove all pollutants by itself. The photocatalyst can be modified and optimized only for the most recalcitrant pollutants while the rest of pollutants might be more easily removed by other cheaper methods (e.g., adsorption, biological degradation).

Controlling the photocatalytic degradation of target substrates in a selective way is a challenging issue since the reactivity of the hydroxyl radical is difficult to control [9,10]. The selective photocatalysis can be approached in various ways. One of them is to modify the surface of the photocatalyst with specific molecules for the selective adsorption of a target substrate. For example, n-octyl-grafted TiO_2 was highly active for the decomposition of 4-nonylphenol [11]. Organosilicone-coated TiO_2 showed better performance for the photocatalytic destruction of the pesticide permathrin [12]. The molecular recognition sites can be introduced on the photocatalyst surface as well. A thin layer of molecular imprinted polymer was coated on the surface of TiO_2, which provided the molecular recognition ability toward the template molecules [13]. Thiolated-cyclodextrin was also employed as the molecular recognition site because it has high affinity for a variety of hazardous contaminants [14]. However, this kind of organic/TiO_2 hybrid photocatalysts suffer from poor stability since the organic component is also degraded through the photocatalytic oxidation [13]. Therefore, the hybrid photocatalysts with all inorganic components are highly desired. For example, titanosilicate molecular

* Corresponding author. Tel.: +82 54 279 2283; fax: +82 54 279 8299.
E-mail address: wchoi@postech.edu (W. Choi).

0304-3894/$ – see front matter © 2011 Elsevier B.V. All rights reserved.
doi:10.1016/j.jhazmat.2011.01.105

sieves such as ETS-4, ETS-10 and TS-1 were employed for the shape-selective photocatalysis [15–17]. However, their photocatalytic activities were low because of the low content of titanium. The core/shell structured inorganic photocatalyst has been also investigated for a similar purpose [18–20]. The titania particles are encapsulated with porous silica shell through which small molecules can penetrate into the titania core while large molecules are rejected at the silica shell.

Zeolites have many advantages as hosts for selective photocatalysis such as the photochemical stability, transparency to UV–visible radiation (above 240 nm), and high/selective adsorption capacity for many substrates [21]. Therefore, the encapsulation of titanium species into the zeolites hosts has been frequently studied for the photocatalytic applications such as the conversion of CO_2 and NO_x [22–24]. Another interesting property of zeolites is the negative charges (balanced by counter cations present in the zeolite pores) carried by the aluminosilicate framework, which results from the substitution of Al^{3+} into the silica structure [25]. In this work, we aimed to develop a zeolite-based hybrid photocatalyst with enhanced selectivity for the degradation of specific charged substrates. FAU-type zeolites with titania encapsulated were prepared and investigated for their photocatalytic activities for the degradation of charged substrates in water. The combination of the photocatalytic activity of titania clusters encapsulated in zeolites, the negative charges of the zeolite framework, and the size of zeolite channel enables the selective degradation of specific cationic substrates in water. This work will provide a model example of the selective photocatalysis applied to water treatment.

2. Materials and methods

2.1. Preparation of catalyst

The encapsulation of titania clusters into zeolites was carried out by successive ion-exchange process followed by heat treatment [22–24]. Two FAU-type zeolites with Si/Al = 5 and 100 (denoted as HFAU1 and HFAU2, respectively) in the proton form were obtained from Tosoh and chosen as the starting materials. First, the proton form of these zeolites was transformed into their sodium form (NaFAU1 and NaFAU2, respectively) by a standard ion-exchange procedure. The zeolite powder was refluxed twice in 1.0 M $NaNO_3$ solutions for 3 h, filtered and then washed with deionized water thoroughly. The obtained powder was kept in an oven at 363 K overnight, and then calcined at 773 K for 5 h. Second, the sodium-type zeolite powder was mixed with 0.05 M aqueous solution of $(Ti{=}O)(NH_4)_2(C_2O_4)_2$ for 12 h at room temperature to incorporate titanium species into zeolites. The sample was filtered and washed with deionized water thoroughly and heated at 373 K overnight to promote the transformation of $Ti{=}O^{2+}$ into TiO_2. The exhaustive water washing was crucial to prevent the physically adsorbed titanium species from aggregating on the external surface of zeolites. The ion exchange process was repeated to get a higher loading of titania. The final samples were calcined at 723 K for 5 h (denoted as TiO_2@FAU1 and TiO_2@FAU2).

The pure TiO_2 powder as a control sample (denoted as syn-TiO_2) was also prepared through a typical sol–gel method (using titanium tetraisoproxide as a precursor). Typically, 4 mL titanium tetraisoproxide was slowly dropped into a 50 mL ethanol and water mixed solution with the volume ratio of 1:1. Then the solution was stirred at room temperature for 5 h, the obtained white powder was filtered and washed with deionized water. Finally, the white powder was kept in an oven overnight and calcined at 723 K for 5 h. A commercial TiO_2 sample, Degussa P25, was also compared as a pure TiO_2.

2.2. Physical and chemical characterization of catalyst

Inductively coupled plasma-atomic emission spectroscopy (ICP-AES, Thermo Jarell Ash IRIS Advantage/1000 Radial ICAP Spectrometer) was used to analyze the composition of the zeolite samples. X-ray photoelectron spectroscopy (XPS, Kratos XSAM 800pci) was carried out to determine the Ti/Si atomic ratio of the titania-loaded zeolites using Ta_2O_5 as reference. The Ar^+ sputtering was done prior to analysis to remove any possible Ti species that may be present on the external surface of zeolites. The powder X-ray diffraction (XRD) patterns were measured on a PANalytical X'Pert diffractomer with an X'Celerator detector. Data were collected with a fixed divergence slit (0.50°) and Soller slits (incident and diffracted = 0.04 rad) and Cu Kα radiation. Diffuse reflectance UV–visible spectra (DRUVS) were recorded using a spectrophotometer (Shimadzu UV-2401PC) with an integrating sphere attachment. $BaSO_4$ was used as the reference. The transmission electron micrographs (TEM) of various samples were recorded using a JEOL JEM-2100F microscope. Zeta potentials of catalyst particles suspended in water were measured using an electrophoretic light scattering spectrophotometer (ELS 8000, Otsuka).

2.3. Photocatalytic activity test and adsorption test

The selective photocatalytic degradation activities were investigated by employing three pairs of oppositely charged organic substrates: RhB (rhodamine B, cationic) and RB19 (reactive blue 19, anionic); AL (aniline, partially protonated as cationic anilinium, $pK_a = 4.7$) and BZ (benzoate, anionic, $pK_a = 4.2$); TMA (tetramethylammonium, cationic) and DCA (dichloroacetate, anionic, $pK_a = 1.3$). The molecular structures of the six substrates are compared in Scheme 1. An aqueous suspension (60 mL) containing 30 mg photocatalyst and single or equimolar mixed substrates was put in a Pyrex cylindrical reaction vessel (100 cm^3 in capacity). The pH of the suspension solution was adjusted to 5.0 ± 0.2 using standard HCl or NaOH solution and then the suspension was stirred for 1.5 h in the dark to allow the adsorption equilibrium of substrates on the catalyst.

A 300-W Xe arc lamp (Oriel) was used as a light source. The light beam was passed through a 10-cm IR water filter and a UV cutoff filter ($\lambda > 300$ nm) and focused onto a cylindrical Pyrex reactor. The reactor was open to the ambient air. Sample aliquots were withdrawn from the reactor intermittently during the illumination. The photocatalytic experiments with a single substrate were carried out using 100 μM RhB or 100 μM RB19 solution. The photocatalytic experiments with equimolar mixed substrates were done using 200 μM AL and 200 μM BZ mixed solution; 200 μM TMA and 200 μM DCA mixed solution.

Adsorption isotherms were obtained as follows. The catalyst powder (5 mg: syn-TiO_2 or TiO_2@FAU1) was added to aqueous solution (10 mL) containing the specific substrate (20–100 μM). The pH of the suspension was adjusted to 5.0 ± 0.2 using standard HCl or NaOH solution. After the mixture was stirred for 1 h in the dark at room temperature, sample aliquots were withdrawn for quantitative analysis. The adsorbed concentrations of substrates were calculated by subtracting the equilibrated concentrations from the initial concentrations.

Quantitative analysis of AL and BZ was done by using a high performance liquid chromatograph (HPLC, Agilent 1100) equipped with a C-18 column and a diode-array detector. TMA and DCA were quantified by using an ion chromatograph (IC, Dionex DX-120) equipped with Dionex IonPac AS14 column and CS 12A column. The concentrations of RhB and RB19 were determined by measuring the maximum absorbance with a UV–visible spectrophotometer (Shimadzu UV-2401PC). The photocatalytic activity was quantified in

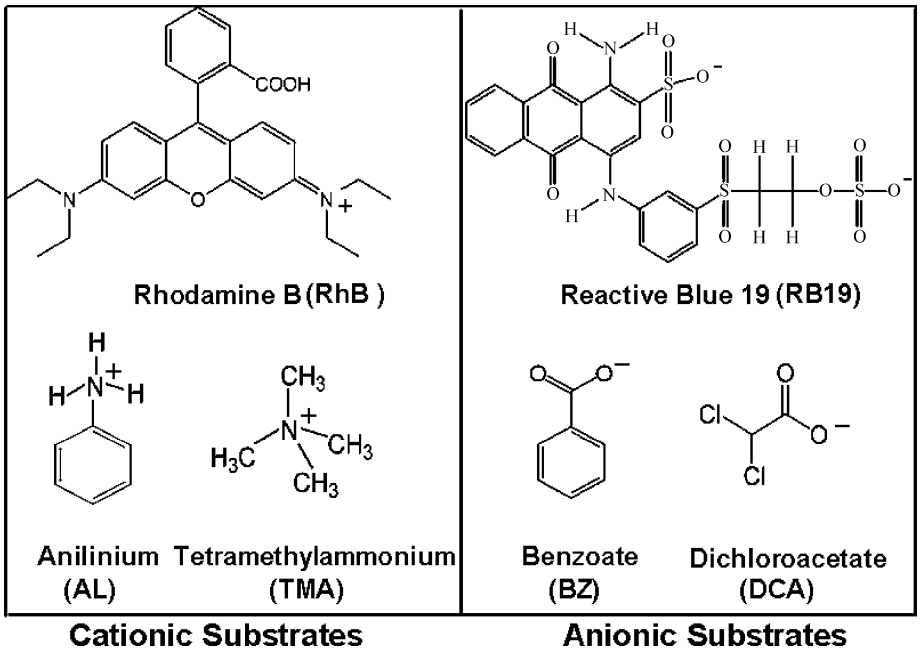

Scheme 1. Molecular structures of the cationic and anionic substrates tested for the photocatalytic degradation in this study.

terms of the apparent first-order rate constant (k) for the removal of various substrates under irradiation.

3. Results and discussion

3.1. Characterization of titania encapsulated into zeolite

It has been well known that the amount of loaded TiO_2 in zeolite is significantly affected by structural parameters of zeolite such as SiO_2/Al_2O_3 ratio, cation type, and topology. In this work, we chose the Si/Al ratio = 5 and 100 of FAU-type zeolite as starting materials. The FAU-type zeolite belongs to the faujasite family and is composing of tetrahedral SiO_4 and AlO_4 building blocks that results in the formation of large cavities with a diameter of ≈1.3 nm. These supercages are connected to each other by tunnels with a widest diameter of ≈0.74 nm. These interconnected tunnels and supercages would provide the space for the loading of TiO_2 molecules inside of zeolite. The elemental composition of the TiO_2@FAU samples was determined by ICP-AES analysis and is summarized in Table 1. As shown in Table 1, TiO_2@FAU1 has a higher Ti content than TiO_2@FAU2 since NaFAU1 with a lower Si/Al ratio has a higher ion exchange capacity than NaFAU2. More $Ti{=}O^{2+}$ ions can be incorporated into NaFAU1 which makes the TiO_2 loading in TiO_2@FAU1 higher [26]. The maximal loading of TiO_2 content calculated by assuming that all sodium ions are exchanged with TiO^{2+} ions is 10.0% and 0.7% in NaFAU1 and NaFAU2, respectively. However, the experimentally determined Ti loadings are a little higher (11.1% and 2.1%, respectively), which might be ascribed to a possibility that TiO^{2+} ions are additionally exchanged with the Bronsted acid sites of the zeolite during the repeated exchange process [27].

To investigate whether the zeolite crystallite was disrupted by the titania loading, the XRD analysis was done as shown in Fig. 1, which confirmed that the ordered zeolite structure was maintained after the titania modification. However, the TiO_2 peaks were not observed probably because the TiO_2 clusters located within the zeolite pores are very small or amorphous. A similar phenomenon was also observed in other study [28]. However, the comparison of DRUVS among NaFAU and TiO_2@FAU samples in Fig. 2a clearly shows the presence of the bandgap absorption induced by titania contained in TiO_2@FAU. Fig. 2b compares the bandgaps of TiO_2 and TiO_2@FAU that were determined from the extrapolated absorption onset. The absorption edges of TiO_2@FAU samples are clearly shifted to shorter wavelengths compared with pure TiO_2 samples. This can be explained by the quantum confinement effect [29] of

Table 1
Elemental composition and estimated bandgaps of prepared photocatalysts.

Sample	Si/Al	Ti/Si[a]	Ti content (TiO_2, %)[a]	Band gap (eV)[b]
syn-TiO_2	–	–	100	3.1
TiO_2@FAU1	5	0.11	11.1	3.5
TiO_2@FAU2	100	0.01	2.1	3.5

[a] Na, Al, Ti elements were analyzed by ICP-AES. Si was calculated from the known Si/Al ratio.
[b] Determined from the absorption onset in the diffuse reflectance spectra expressed in the Kubelka–Munk (KM) function (see Fig. 2b).

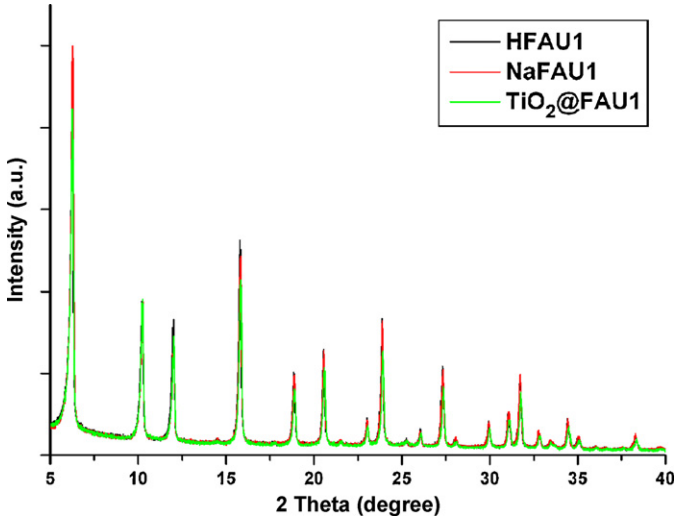

Fig. 1. XRD spectra of original zeolite (HFAU1); after sodium exchange modification (NaFAU1); after titanium loading (TiO_2@FAU1).

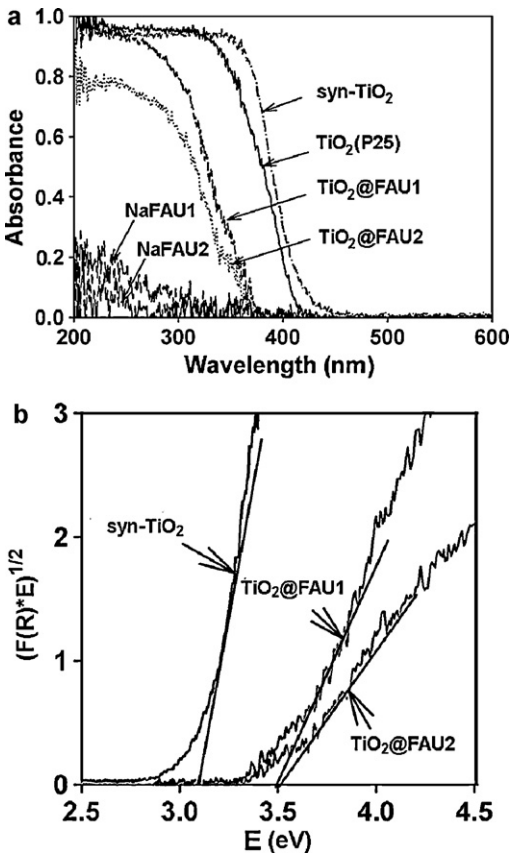

Fig. 2. (a) Diffuse reflectance UV–visible spectra (DRUVS) of various catalyst samples, (b) conversion of the DRUVS into the plot of Kubelka–Munk function versus photon energy ($[F(R) \times E]^{1/2}$ vs E).

titania clusters within the zeolite pores and indicates that the size of titania nanoparticles in the zeolites is smaller than that of P25 and syn-TiO_2. There is no significant change in the bandgap for TiO_2@FAU1 and TiO_2@FAU2, indicating that the size of TiO_2 clusters in the interior of zeolites might be similar. The bandgap of the quantum-sized TiO_2 nanoparticles is related with their radius through the following equation [30,31]:

$$\Delta E_g = \frac{h^2}{8R^2\mu} - \frac{1.8e^2}{\varepsilon R} \quad (1)$$

where R is the radius of the particle; μ is the reduced mass of the exciton = $1.63m_e$ for TiO_2; ε is the dielectric constant of the semiconductor = 184 for TiO_2.

The diameter of titania clusters determined by Eq. (1) is 1.8 nm for TiO_2@FAU1 and TiO_2@FAU2, which is not so large compared to the diameter (1.3 nm) of supercages in FAU-type zeolites [32], suggesting that most (if not all) TiO_2 clusters are present in intrazeolitic cavities. The XRD size of syn-TiO_2 particles is estimated to be about 16 nm according to Scherrer's equation.

Fig. 3 shows the TEM images of NaFAU1 and TiO_2@FAU1. It can bee seen that the TiO_2 clusters exist between the lattice planes of NaFAU1, whereas none of them are observed on the external surface of the zeolite crystals. We were not able to accurately determine the size of TiO_2 clusters from the TEM image due to their overlapping nature within the zeolite lattice. The EDX mapping analysis (see Fig. 4) shows that Ti elements are distributed over the whole zeolite framework. TiO_2@FAU1 shows much higher titanium distribution signal in Fig. 4c than that of TiO_2@FAU2 in Fig. 4f, which is consistent with the higher Ti loading of TiO_2@FAU1 (see Table 1).

To further probe the distribution of Ti within the zeolites, the elemental ratio of Ti/Si in TiO_2@FAU samples was analyzed by XPS along with Ar^+ bombardment (see Fig. 5). The profile of the Ti/Si atomic ratio remained relatively constant throughout the ion sputtering time, which indicates that the Ti elements are uniformly distributed within the zeolites. The sputtering time of 200 s corresponds to the etching depth of 10 nm, which should be long enough to etch out the external surface of the zeolites. The observation that the Ti/Si ratio did not vary much during this sputtering process implies that the titania species are not loaded on the external surface of the zeolites. This is consistent with what TEM images in Fig. 3 show. If the titania nanoparticles were aggregated on the external surface of the zeolites, the Ti/Si ratio should decrease rapidly with the sputtering time. The XPS Ti/Si ratios are around 0.04($\pm$0.005) and 0.007($\pm$0.003) for TiO_2@FAU1 and TiO_2@FAU2, respectively, which are lower than those obtained from the ICP analysis (see Table 1). This indicates that the titanium content in the surface region of the zeolites is lower than in the bulk region since XPS analyzes the surface region only. As TEM images in Fig. 3 show, the titania clusters are well buried within the porous framework of the zeolites. Both TEM and XPS analyses support that TiO_2 clusters are mainly located in the interior of the zeolites.

The surface charges of TiO_2 and TiO_2@FAU samples were analyzed by measuring the zeta potential as shown in Fig. 6. While the point of zero zeta potentials (PZZP) of pure TiO_2 (P25 and syn-TiO_2) are in the range of 5.5–6.5, those of TiO_2@FAU are significantly shifted to lower pH (about 2) because of the negative charges of the zeolite framework. As a result, the surface of TiO_2@FAU carries dominant negative charges at pH > 2 under which condition cationic substrates should be attracted.

3.2. Photocatalytic activities of TiO_2@FAU

The adsorption of substrates on the photocatalyst is an important factor that affects the photocatalytic activity. The adsorption isotherms of various substrates were determined with syn-TiO_2 and TiO_2@FAU1 samples. As shown in Fig. 7a, the cationic substrates such as RhB (rhodamine B), TMA (tetramethylammonium) and AL (anilinium) are strongly adsorbed onto TiO_2@FAU1, while the anionic substrates such as RB19 (reactive blue 19), DCA (dichloroacetate) and BZ (benzoate) are hardly adsorbed onto TiO_2@FAU1. This phenomenon could be clearly explained as the electrostatic attraction or repulsion between the negatively charged zeolite framework and the charged substrates controls the adsorption behavior. The TiO_2@FAU1 shows the largest adsorption toward TMA since it is the smallest molecule among the tested cationic substrates and thus easier to diffuse into the zeolite pores. RhB, being the largest cationic substrate, exhibits the lowest adsorption on TiO_2@FAU1 since its penetration into the zeolite pores is hindered. It is assumed that a significant fraction of adsorbed RhB molecules are located on the external surface of zeolite. On the other hand, the adsorption characteristics of syn-TiO_2 (pure TiO_2) (shown in Fig. 7b) are markedly different from those of TiO_2@FAU1. The syn-TiO_2 shows lower adsorption affinity toward both cationic and anionic substrates except the dye molecules. Since the pH of zero point of charge (pH_{ZCP}) of TiO_2 is around 5.5–6.5 (see Fig. 6), TiO_2 at near neutral condition (pH 5 in this case of adsorption) should have weak electrostatic interaction with and little affinity toward the charged substrates. The bulky dye molecules (RhB and RB19) of which adsorption into the zeolite pores are hindered are more favorably adsorbed on syn-TiO_2. It is noted that the relative affinity of syn-TiO_2 toward RhB and RB19 is reverse to that of TiO_2@FAU1. RB19 is not adsorbed on TiO_2@FAU1 at all but its adsorption on syn-TiO_2 shows the highest affinity among all test substrates. The reactive functional groups in RB19 seem to have a stronger interaction with the surface of TiO_2. Comparing the adsorption isotherms

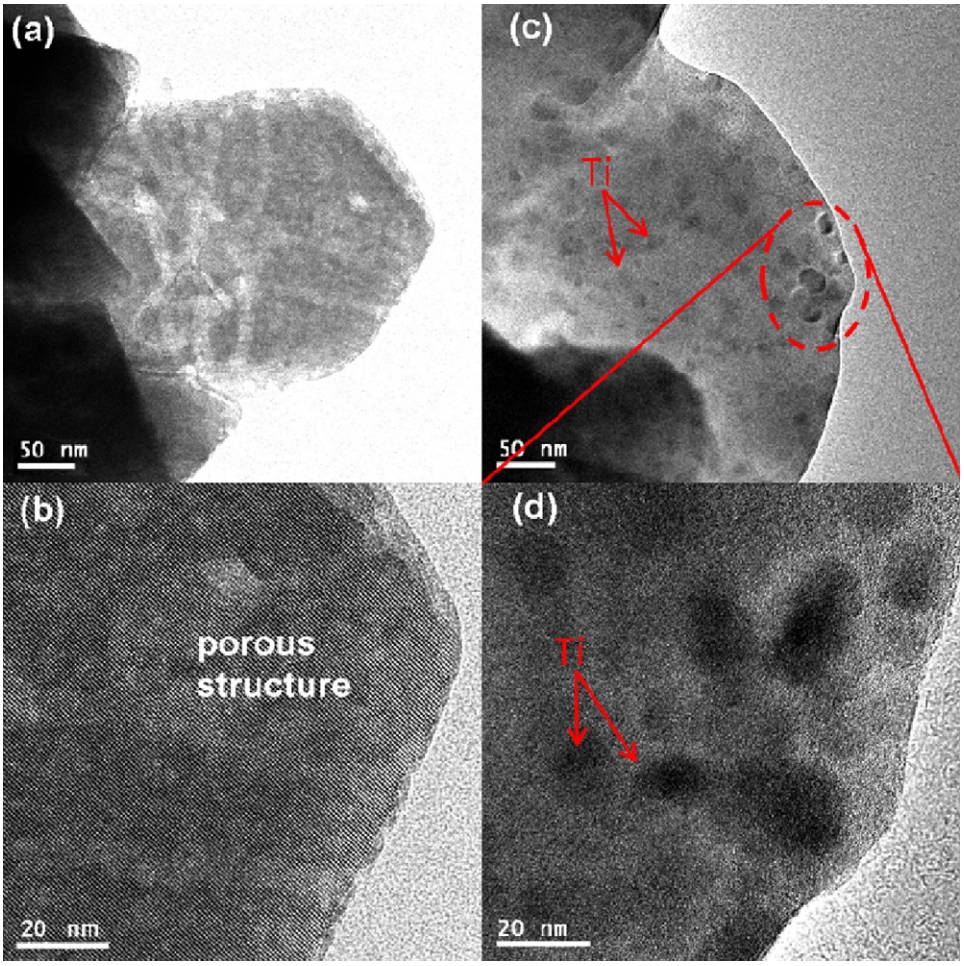

Fig. 3. TEM images of various samples: NaFAU1 (a) and (b); TiO_2@FAU1 (c) and (d).

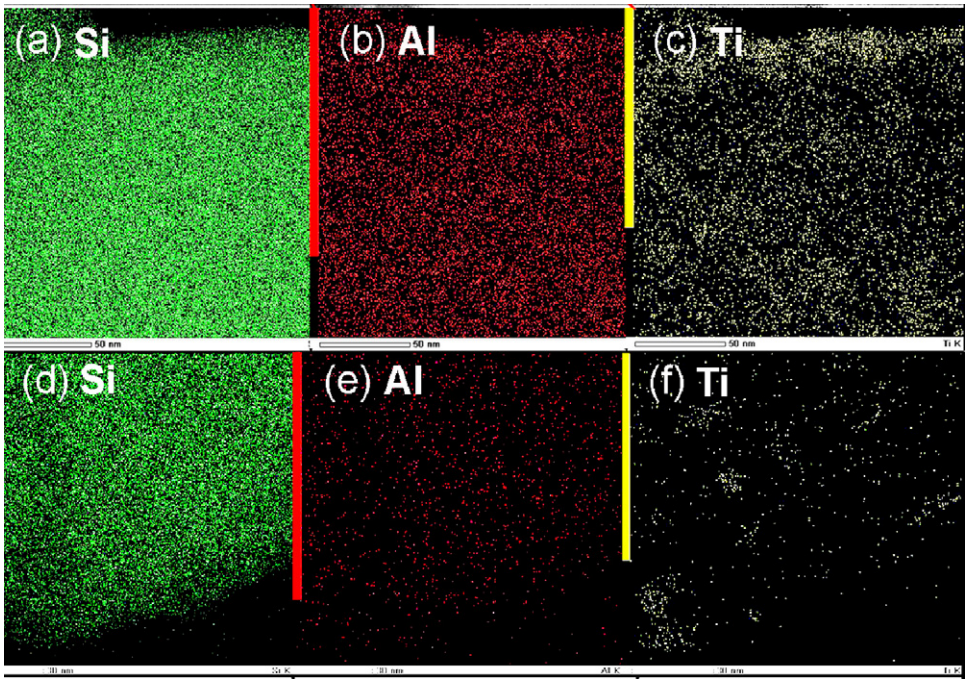

Fig. 4. EDX elemental mapping images of TiO_2@FAU1 sample: (a) Si, (b) Al, (c) Ti and TiO_2@FAU2 sample: (d) Si, (e) Al, (f) Ti.

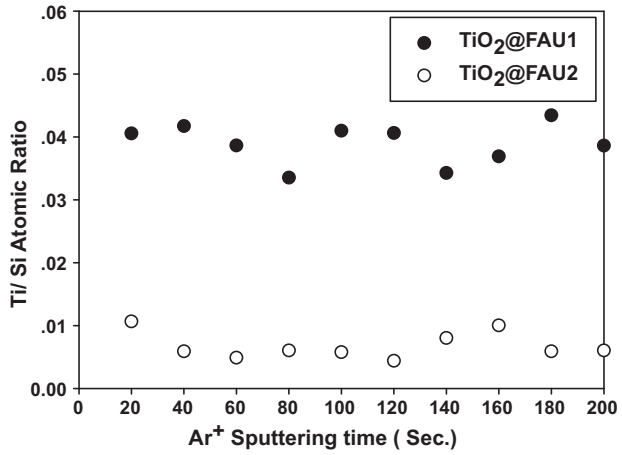

Fig. 5. XPS depth profile of TiO_2@FAU1 and TiO_2@FAU2 samples (Ar^+ sputtering distance from 0 to 10 nm inside).

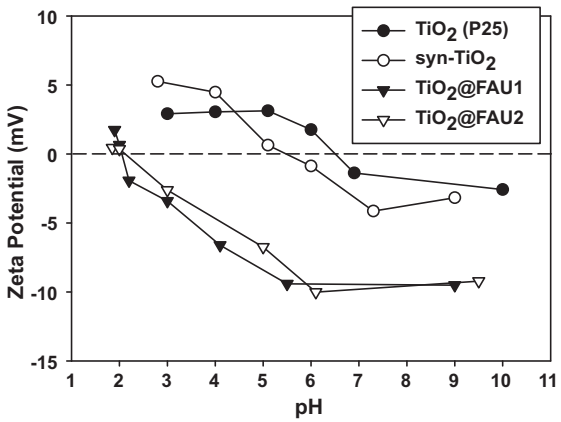

Fig. 6. Zeta potentials of various catalyst samples suspended in water as a function of pH ([TiO_2(P25)] = 2 mg/L, [others] = 20 mg/L, containing 0.05 mM $NaNO_3$ electrolyte).

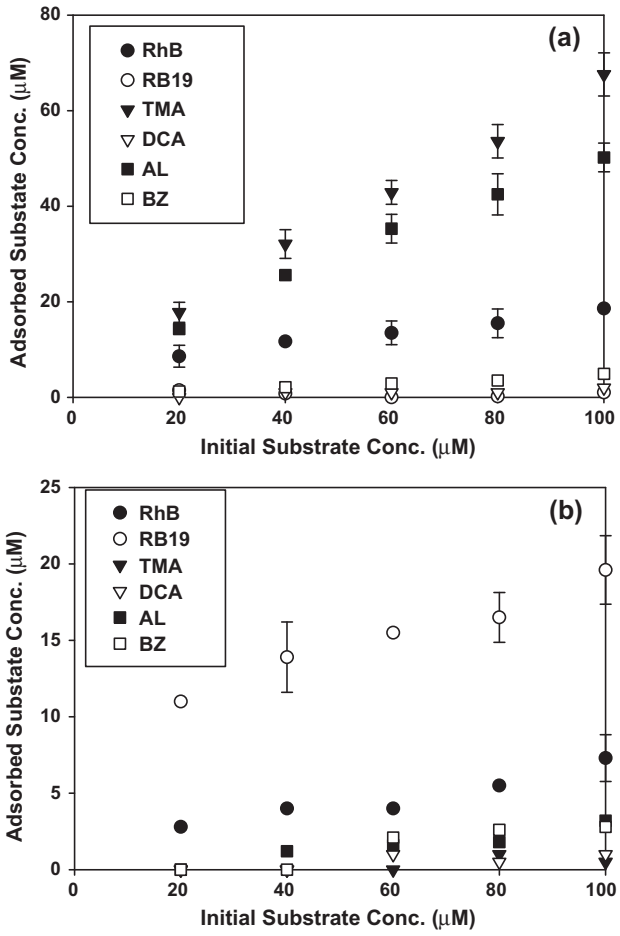

Fig. 7. Adsorption isotherms of various substrates on (a) TiO_2@FAU1 and (b) syn-TiO_2 suspended in water ([catalyst] = 0.5 g/L, pH 5.0 ± 0.2). Filled symbols represent the cationic substrates and open symbols the anionic substrates.

of TiO_2@FAU1 and syn-TiO_2, it is clear that TiO_2@FAU1 exhibits the charge-selective adsorption characteristics, which should affect the photocatalytic selectivity.

The charge-selective photocatalytic activities were tested for the above three pairs of oppositely charged substrates. The photocatalytic degradation of single or mixed substrates with TiO_2@FAU was carried out and compared with syn-TiO_2 (as a control) under the identical experimental condition. The photocatalytic activities of hybrid zeolite catalysts are expressed in terms of the first-order rate constant (k) for the removal of various charged substrates and compared with that of pure TiO_2 (syn-TiO_2) (see Table 2). In all cases, the removal of substrates by direct photolysis (without catalyst) was negligible. For the degradation of dyes (RhB and RB19), TiO_2@FAU2 shows more than 50 times higher photocatalytic activity for cationic RhB than anionic RB19, whereas syn-TiO_2 shows comparable activities for RhB and RB19 under the same reaction condition. This is consistent with the adsorption behavior shown in Fig. 7a. The observation that the degradation of RhB (largest cation) on TiO_2@FAU is comparable to that on syn-TiO_2 is interesting. RhB molecules, which are too big to freely diffuse into the zeolite cavity, are mostly adsorbed on the external surface of the zeolites through the electrostatic attraction whereas the active TiO_2 clusters are in the interior of zeolite, not on the external surface. Therefore, RhB molecules may not be in the direct contact with TiO_2 clusters. A plausible degradation mechanism is the photocatalytic oxidation that is mediated by the OH radicals migrating from the interior TiO_2 clusters to the external surface [33]. In the degradation process of RhB, we observed some blue shift in the main absorbance band (centered at 554 nm), which was insignificant with syn-TiO_2 but measurable with TiO_2@FAU. This implies that the degradation mechanism is different. The blue shift in the RhB absorption band indicates that it undergoes the N-de-ethylation more preferentially on TiO_2@FAU [34]. On the other hand, the anionic RB19 was hardly adsorbed by zeolites and thus degraded with much slower rate. In general, substrates can be adsorbed not only on the external surface of zeolite but also on the inner titania particles depending on their size and charge. Therefore, both holes and migrating radical species should be involved as oxidants. The photocatalytic

Table 2
Photocatalytic degradation rate constant for the removal of various charged substrates.

Catalyst	First-order rate constant, k (10^{-3} min^{-1})					
	Cationic substrate			Anionic substrate		
	RhB	AL	TMA	RB19	BZ	DCA
syn-TiO_2	4.84	3.5	0.74	8.89	3.41	35.57
TiO_2@FAU1	5.77	3.21	3.55	0.86	0.46	1.95
TiO_2@FAU2	3.20	1.03	1.11	0.06	0.64	2.27

[Catalyst] = 0.5 g/L; pH 5.0 ± 0.2; the single substrate experiments were carried out using 100 μM RhB or 100 μM RB19 solution; the equimolar mixed substrates experiments were done using 200 μM AL and 200 μM BZ mixed solution; 200 μM TMA and 200 μM DCA mixed solution.

degradation mechanism and the kind of major oxidants can be different for each substrate [5]. In addition, it should be noted that a variety of intermediates with different charge characteristics can be produced during the degradation process and the selectivity of a photocatalyst for the intermediates can be different from that for the parent substrate. In this study, we focused only on the removal of parent substrates. In case there is significant selectivity difference between a parent substrate and intermediates, the photocatalytic activity for the removal of a parent substrate can be very different from that for the removal of total organic carbon.

With the mixed substrates (AL and BZ, TMA and DCA), the selective photodegradation was also observed. TiO_2@FAU samples showed much faster degradation for cationic AL than anionic BZ. As for the case of TMA and DCA mixture, the relative photocatalytic degradation activity for TMA and DCA is reversed between syn-TiO_2 and TiO_2@FAU samples. Compared with syn-TiO_2, the photocatalytic degradation of TMA was enhanced with TiO_2@FAU whereas that of DCA was greatly inhibited with TiO_2@FAU. The diffusion of smaller cationic AL and TMA molecules into the zeolite pores (with negative charge) facilitates the photocatalytic degradation on the interior TiO_2 whereas the repulsion of anionic BZ and DCA retards their degradation.

Fig. 8a compares the photocatalytic activities for each substrate in terms of the relative ratio $R = [k(TiO_2@FAU)/k(TiO_2)]$. R refers to the relative rate with respect to the degradation rate on pure titania. The comparison between the cationic and anionic substrates clearly shows that the photocatalytic activities for the degradation of cationic substrates on TiO_2@FAU are consistently higher than those for anionic substrates. It should be noted that R values of anionic substrates are markedly lower than unity ($R_{anion} \ll 1$). This indicates that the electrostatic interaction between the substrates and the negatively charged zeolite framework selectively controls the photocatalytic activity of the encapsulated TiO_2 nanoparticles depending on the charge of the substrates. The electrostatic attraction between TiO_2@FAU and cationic substrates should facilitate the photocatalytic degradation. On the other hand, the electrostatic repulsion between anionic substrates and TiO_2@FAU markedly inhibits their degradation in comparison with TiO_2 nanoparticles. As a result, the photocatalytic degradation on the hybrid photocatalysts is much favored for cationic substrates among the cationic and anionic mixture. Incidentally, the size-selective control by the zeolitic pore is also observed. Among the three cationic substrates (RhB, TMA, and AL), the relative enhancement in the degradation rate (R value) is the highest with TMA, the smallest cation, which should diffuse most easily into the titania clusters embedded within the zeolite pores.

The activity comparison of TiO_2@FAU and syn-TiO_2 in terms of the apparent rate constant, k (10^{-3} min^{-1}), however, is not based on the same mass of active TiO_2 component, but on the total mass of the hybrid catalyst. TiO_2@FAU catalyst contains only a fraction of active TiO_2 content out of the total mass (see Table 1). Therefore, the charge-selective photocatalytic activity of TiO_2@FAU is much higher when the photocatalytic activity for each substrate is expressed in terms of the relative ratio $R_n = k_n(TiO_2@FAU)/k_n$(syn-TiO_2) that is based on the rate constant normalized by TiO_2 mass [k_n, min^{-1} (g TiO_2)$^{-1}$] (see Fig. 8b). The comparison between the cationic and anionic substrates clearly shows that the relative rates for the degradation of cationic substrates on TiO_2@FAU are markedly higher compared with those of anionic substrates ($R_{cation} \gg R_{anion}$) (Fig. 8b). On the other hand, the normalized degradation activities for cationic substrates on TiO_2@FAU are notably higher than those of unconfined TiO_2 nanoparticles ($R_{cation} \gg 1$), which indicates that the TiO_2 clusters encapsulated into zeolites are much more selective than pure titania for the photocatalytic degradation of cationic compounds. Among the cationic substrates, TMA showed the highest R_n value, which reconfirms the size-dependent selectivity of TiO_2@FAU.

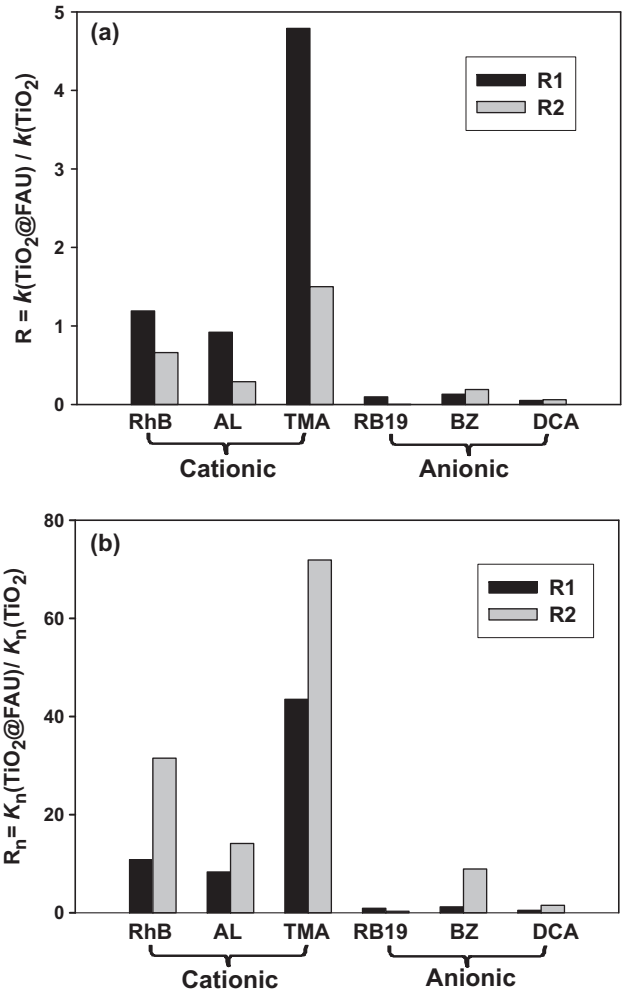

Fig. 8. Photocatalytic activities of various samples for the degradation of cationic substrates: RhB, AL, TMA; anionic substrates: RB19, BZ, DCA. (a) The activities of photocatalytic degradation are expressed in terms of the relative ratio: $R_1 = [k(TiO_2@FAU1)/k(TiO_2)]$, $R_2 = [k(TiO_2@FAU2)/k(TiO_2)]$ based on the apparent rate constant (k, 10^{-3} min^{-1}); (b) the alternative expression of the relative ratio: $(R_1)_n = [k_n(TiO_2@FAU1)/k_n(TiO_2)]$, $(R_2)_n = [k_n(TiO_2@FAU2)/k_n(TiO_2)]$ based on the apparent rate constant normalized by TiO_2 mass [k_n, min^{-1} (g TiO_2)$^{-1}$].

4. Conclusions

The encapsulation of titania clusters into FAU-type zeolite pores was obtained through ion-exchange process followed by heat treatment. The FAU-type zeolite with lower Si/Al ratio shows the higher titanium loading due to its higher ion-exchange capacity. The titania clusters are mainly located within the framework of zeolite, while no TiO_2 nanoparticles aggregates could be found on the external surface of zeolite. The hybrid zeolite/TiO_2 photocatalysts were fully characterized using various analytical methods and confirmed that smaller titania clusters are well dispersed within the zeolite pores. The charge-selective photocatalytic degradation of charged aquatic pollutants was successfully achieved by using the prepared hybrid photocatalysts. The electrostatic attraction of cationic substrates such as RhB, TMA, and AL by the negative charged framework of zeolite facilitated their photocatalytic degradation on TiO_2 clusters within the zeolite, whereas the electrostatic repulsion of anionic substrates such as RB19, BZ, and DCA hindered the photocatalytic degradation. The hybrid photocatalyst exhibited the

size-dependent selectivity as well. Among the cationic substrates, the smallest cations (TMA) were most preferentially degraded. The hybrid photocatalysts with enhanced selectivity for the degradation of targeted substrates may provide a useful strategy for the photocatalytic treatment of polluted water. For example, the photocatalytic technology for practical water treatment may not be cost-effective when it aims to remove all kind of pollutants by itself. The contaminated water contains a wide variety of pollutants whose degradability (physicochemical or biological) highly vary. The selective photocatalysis may target the most recalcitrant pollutant (e.g., TMA from the semiconductor industry wastewater [33]) and the rest of pollutants can be removed by less costly process such as the conventional biological water treatment.

Acknowledgements

This work supported by KOSEF NRL program (No. R0A-2008-000-20068-0), KOSEF EPB center (Grant No. R11-2008-052-02002), and KCAP (Sogang Univ.) funded by MEST through NRF (NRF-2009-C1AAA001-2009-0093879).

References

[1] M.R. Hoffmann, S.T. Martin, W. Choi, D.W. Bahnemann, Environmental applications of semiconductor photocatalysis, Chem. Rev. 95 (1995) 69–96.
[2] S. Bangkedphol, H.E. Keenan, C.M. Davidson, A. Sakultantimetha, W. Sirisaksoontorn, A. Songsasen, Enhancement of tributyltin degradation under natural light by N-doped TiO_2 photocatalyst, J. Hazard. Mater. 184 (2010) 533–537.
[3] Y. Ku, P.C. Chiu, Y.C. Chou, Decomposition of aniline in aqueous solution by UV/TiO_2 process with applying bias potential, J. Hazard. Mater. 184 (2010) 533–537.
[4] W. Choi, Pure and modified TiO_2 photocatalysts and their environmental applications, Catal. Surv. Asia 10 (2006) 16–28.
[5] J. Ryu, W. Choi, Substrate-specific photocatalytic activities of TiO_2 and multiactivity test for water treatment application, Environ. Sci. Technol. 42 (2008) 294–300.
[6] J. Kim, J. Lee, W. Choi, Synergic effect of simultaneous fluorination and platinization of TiO_2 surface on anoxic photocatalytic degradation of organic compounds, Chem. Commun. (2008) 756–758.
[7] G. Marcì, A. Sclafani, V. Augugliaro, L. Palmisano, M. Schiavello, Influence of some aromatic and aliphatic compounds on the rate of photodegradation of phenol in aqueous suspensions of TiO_2, J. Photochem. Photobiol. A: Chem. 89 (1995) 69–74.
[8] A. Di Paola, E. Garcıĭa-López, S. Ikeda, G. Marcı, B. Ohtani, L. Palmisano, Photocatalytic degradation of organic compounds in aqueous systems by transition metal doped polycrystalline TiO_2, Catal. Today 75 (2002) 87–93.
[9] S.H. Zhan, D.R. Chen, X.L. Jiao, Y. Song, Mesoporous TiO_2/SiO_2 composite nanofibers with selective photocatalytic properties, Chem. Commun. (2007) 2043–2045.
[10] S. Ikeda, Y. Ikoma, H. Kobayashi, T. Harada, T. Torimoto, B. Ohtani, M. Matsumura, Encapsulation of titanium oxide particles in hollow silica for size-selective photocatalytic reactions, Chem. Commun. (2007) 3753–3755.
[11] K. Inumaru, M. Murashima, T. Kasahara, S. Yamanaka, Enhanced photocatalytic decomposition of 4-nonylphenol by surface-organografted TiO_2: a combination of molecular selective adsorption and photocatalysis, Appl. Catal. B 52 (2004) 275–280.
[12] H. Hidaka, K. Nohara, J. Zhao, N. Serpone, E. Pelizzetti, Photo-oxidative degradation of the pesticide permethrin catalysed by irradiated TiO_2 semiconductor slurries in aqueous media, J. Photochem. Photobiol. A: Chem. 64 (1992) 247–254.
[13] X.T. Shen, L.H. Zhu, G.X. Liu, H.W. Yu, H.Q. Tang, Enhanced photocatalytic degradation and selective removal of nitrophenols by using surface molecular imprinted titania, Environ. Sci. Technol. 42 (2008) 1687–1692.
[14] S. Ghosh-Mukerji, H. Haick, M. Schvartzman, Y. Paz, Selective photocatalysis by means of molecular recognition, J. Am. Chem. Soc. 123 (2001) 10776–10777.
[15] P. Calza, C. Paze, E. Pelizzetti, A. Zecchina, Shape-selective photocatalytic transformation of phenols in an aqueous medium, Chem. Commun. (2001) 2130–2131.
[16] Y. Shiraishi, N. Saito, T. Hirai, Titanosilicate molecular sieve for size-screening photocatalytic conversion, J. Am. Chem. Soc. 127 (2005) 8304–8306.
[17] S. Usseglio, P. Calza, A. Damin, C. Minero, S. Bordiga, C. Lamberti, E. Pelizzetti, A. Zecchina, Tailoring the selectivity of Ti-based photocatalysts (TiO_2 and microporous ETS-10 and ETS-4) by playing with surface morphology and electronic structure, Chem. Mater. 18 (2006) 3412–3424.
[18] K. Inumaru, T. Kasahara, M. Yasui, S. Yamanaka, Direct nanocomposite of crystalline TiO_2 particles and mesoporous silica as a molecular selective and highly active photocatalyst, Chem. Commun. (2005) 2131–2133.
[19] S. Wang, T. Wang, W.X. Chen, T.R. Hori, Phase-selectivity photocatalysis: a new approach in organic pollutants' photodecomposition by nanovoid core(TiO_2)/shell(SiO_2) nanoparticles, Chem. Commun. (2008) 3756–3758.
[20] S. Ikeda, H. Kobayashi, Y. Ikoma, T. Harada, T. Torimoto, B. Ohtani, M. Matsumura, Size-selective photocatalytic reactions by titanium oxide coated with a hollow silica shell in aqueous solutions, Phys. Chem. Chem. Phys. 9 (2007) 6319–6326.
[21] A. Corma, H. Garcia, Zeolite based photocatalysts, Chem. Commun. (2004) 1443–1459.
[22] M. Kitano, M. Matsuoka, M. Ueshima, M. Anpo, Recent developments in titanium oxide-based photocatalysts, Appl. Catal. A 325 (2007) 1–14.
[23] M. Alvaro, E. Carbonell, P. Atienzar, H. Garcia, A novel concept for photovoltaic cells: clusters of titanium dioxide encapsulated within zeolites as photoactive semiconductors, ChemPhyChem 7 (2006) 1996–2002.
[24] P. Atienzar, S. Valencia, A. Corma, H. Garcia, Titanium-containing zeolites and microporous molecular sieves as photovoltaic solar cells, ChemPhysChem 8 (2007) 1115–1119.
[25] M.N. Chretien, Supramolecular photochemistry in zeolites: from catalysts to sunscreens, Pure Appl. Chem. 79 (2007) 1–20.
[26] X.S. Liu, K.K. Iu, J.K. Thomas, Encapsulation of TiO_2 in zeolite Y, Chem. Phys. Lett. 195 (1992) 163–168.
[27] H. Chen, A. Matsumoto, N. Nishimiya, K. Tsutsumi, Preparation and characterization of TiO_2 incorporated Y-zeolite, Colloid Surf. A 57 (1999) 295–305.
[28] G. Cosa, M. Galletero, L. Fernandez, F. Marquez, H. Garcia, J.C. Scaiano, Tuning the photocatalytic activity of titanium dioxide by encapsulation inside zeolites exemplified by the cases of thianthrene photooxygenation and horseradish peroxidase photodeactivation, New J. Chem. 26 (2002) 1448–1455.
[29] M.V. Rama Krishna, R.A. Friesner, Quantum confinement effects in semiconductor clusters, J. Chem. Phys. 95 (1991) 8309–8322.
[30] L.E. Brus, Electronic wave functions in semiconductor clusters: experiment and theory, J. Phys. Chem. 90 (1986) 2555–2560.
[31] W. Choi, A. Termin, M.R. Hoffmann, The role of metal-ion dopants in quantum-sized TiO_2: correlation between photoreactivity and charge–carrier recombination dynamics, J. Phys. Chem. 98 (1994) 13669–13679.
[32] A.N. Fitch, H. Jobic, A. Renouprez, Localization of benzene in sodium–Y zeolite by powder neutron diffraction, J. Phys. Chem. 90 (1986) 1311–1318.
[33] S. Kim, W. Choi, Kinetics and mechanisms of photocatalytic degradation of $(CH_3)_nNH_{4-n}^+(0 \le n \le 4)$ in TiO_2 suspension: the role of OH radicals, Environ. Sci. Technol. 36 (2002) 2019–2025.
[34] H. Park, W. Choi, Photocatalytic reactivities of nafion-coated TiO_2 for the degradation of charged organic compounds under UV or visible light, J. Phys. Chem. B 109 (2005) 11667–11674.